Annals of Nuclear Energy 177 (2022) 109302

Contents lists available at ScienceDirect

Annals of Nuclear Energy

journal homepage: www.elsevier.com/locate/anucene

Research on a localization method of multiple unknown gamma radioactive sources

Xulin Hu [a], Jianwen Huo [a,*], Junling Wang [b], Li Hu [a], Yufeng Xiao [a]

[a] School of Information Engineering, Southwest University of Science and Technology, Mianyang 621010, China
[b] School of National Defense Science, Southwest University of Science and Technology, Mianyang 621010, China

ARTICLE INFO

Article history:
Received 5 April 2022
Received in revised form 19 June 2022
Accepted 20 June 2022

Keywords:
Multiple unknown radioactive sources
Localization
Convolutional neural network
Self-avoiding walk

ABSTRACT

Accidental loss of radioactive sources will pose a great threat to social security and the national economy, and may cause mass casualties and serious social panic. This paper explores a localization method of multiple unknown radioactive sources based on the convolutional neural network (CNN) algorithm to search for lost or unknown radioactive sources. The energy deposition distribution of multiple gamma (γ) radioactive sources in an area is obtained by Geant4 simulation. Additionally, the energy deposition values in the area are randomly collected by using the self-avoiding walk (SAW) algorithm, and three datasets of training, validation and test are constructed. The collected data can be trained and analyzed by a convolutional neural network to determine the locations of radioactive sources. Further, in order to verify the performance of the algorithm, group experiments are carried out, including the existence of obstacles in the area, the length of obstacles, the number of radioactive sources, etc. The experimental results show that the respective locations of two radioactive sources can be predicted with 89% accuracy by only collecting 10 energy deposition values in the area. In the case of complex obstacles, the accuracy can reach 68%. Besides, the respective locations of three radioactive sources can be predicted with at least 86% accuracy in a restricted area. The experimental results show the feasibility of the proposed method for the localization of multiple unknown radioactive sources.

1. Introduction

For more than half a century, nuclear energy has played an important role in optimizing the energy structure, ensuring energy security, promoting the reduction of pollution and addressing climate change. According to incomplete statistics, there are currently 457 nuclear reactors in operation worldwide, with a total installed capacity of 400 million MW. However, in the process of nuclear energy and nuclear technology development, if a nuclear accident occurs, it will pose a serious threat to social security and the national economy, and may cause mass casualties and serious social panic. According to statistics from the International Atomic Energy Agency, up to now, more than 3600 nuclear accidents and theft of radioactive materials have been confirmed by the Illegal Traffic Database (ITDB) (IAEA Incident and Trafficking Database, 2020). Therefore, how to quickly and accurately locate the radioactive source by acquiring radiation data in the environment is an important security issue in the application of nuclear technology.

Although researchers have been investigating how to search for and locate lost radioactive sources by using various methods, locating them remains a challenging task. The main difficulties come from: (1) If the lost or stolen radioactive sources are searched manually, it will take a long time and present serious health risk to operators (Kamiya et al., 2015). (2) The area where the radioactive source is lost may have walls that block the radiation signal and affect the estimation of the radioactive source location (Chao et al., 2019). (3) When there are two or more radioactive sources in an area simultaneously, the radiation signals from multiple radioactive sources will interfere with each other, which will have a great impact on the radiation measurements (Morelande et al., 2007). Therefore, this paper combines the convolutional neural network (CNN) with the self-avoiding walk (SAW) to design a localization method for multiple γ radioactive sources. The main contributions of this paper are as follows: (1) The loss of the radioactive source is a random event, which may be single or multiple. In this paper, the energy deposition distribution of multiple radioactive sources at various locations in the area is simulated by Geant4, so as to obtain the approximate energy deposition distribution of radioactive sources in real life. (2) Considering the uncertainty of the location of radiation detection during the

* Corresponding author.
E-mail address: huojianwen2008@hotmail.com (J. Huo).

https://doi.org/10.1016/j.anucene.2022.109302
0306-4549/

radioactive source search, the SAW algorithm is used to collect the energy deposition values at different locations. (3) Combined with the energy deposition values collected by the SAW algorithm, a localization method for multiple radioactive sources based on multi-channel CNN is proposed. Experiments show that the proposed method can quickly locate multiple unknown radioactive sources in the radiation environment with complex obstacles.

The structure of this paper is as follows: Section 2 introduces the current research methods of radioactive source localization, and compares the differences between the method proposed in this paper and others. Section 3 indicates the radioactive source detection task and describes the localization method combining SAW and CNN algorithms in detail. Section 4 analyzes the accuracy of the proposed method for estimating the location of the radioactive source under different geometric conditions. Section 5 summarizes the paper and discusses future research directions.

2. Related work

Traditional radioactive source localization methods typically utilize nuclear radiation detectors to measure radiation at multiple points in the area, and then build a sensor network to estimate the location and intensity of radioactive source (Chin et al., 2008; Liu, 2010). Gunatilaka et al., devised a geometric method to estimate the location and intensity of a single gamma radiation source by measuring radiation values in the environment (Gunatilaka et al., 2007). Howse et al., studied the problem of tracking the location of radioactive sources in real time using the least squares method (Howse et al., 2001). Another kind of localization algorithm was based on maximum likelihood estimation. Collecting a large amount of radiometric data from multiple sensors, the maximum likelihood estimation method can estimate the number of radioactive sources and source parameters (Bai et al., 2007; Chandy et al., 2008). However, the maximum likelihood estimation method was not applicable when more than two radioactive sources were present simultaneously in an area. The Bayesian estimation method was also commonly used to estimate the source parameters which were obtained by solving the posterior probability distribution (Liu et al., 2011; Morelande and Ristic, 2009).

In addition, the method for locating radioactive sources by a single robot or multi-robot cooperative search has been investigated, which was suitable for automatically searching for a single radioactive source in an unobstructed environment (Huo et al., 2020; Ling et al., 2022). A method using particle filtering to handle multimodal problems in a mixed radiation field with sparse measurements has also been proposed (Gao et al., 2018). Compton gamma camera has also been studied to locate radioactive sources, which was able to map the spatial distribution of radiation in cluttered 3D settings by recording information such as the number and direction of incident gamma photons (Lee et al., 2018). It was worth noting that a method for localizing tagged items in 3D space with a mobile robot has also been proposed, which was similar to the problem of source localization (Liu et al., 2013; Liu et al., 2015).

Nowadays deep learning and reinforcement learning have been applied to radioactive waste classification, radionuclide identification, and radioactive source search (Hata et al., 2015; Bobin et al., 2016; Fathi and Masoudi, 2021; Liu and Abbaszadeh, 2019). For example, the rapid classification of uranium waste through support vector machines (Hata et al., 2015) and the real-time identification of various radionuclides using spiking neural networks (Bobin et al., 2016), etc. In Fathi and Masoudi (2021), the energy deposition distribution of gamma source on the ground was simulated, and then the location of a single gamma source was estimated by the method of deep learning. In Liu and Abbaszadeh (2019), by continuously updating the radiation measurement values, the number of measurements, and the current measurement position into the neural network for training, the network was going to predict the next travel direction until the radioactive source was searched. The studies of (Fathi and Masoudi, 2021; Liu and Abbaszadeh, 2019) provide valuable ideas for the localization method of multiple gamma radioactive sources in this paper. But this paper differs from (Fathi and Masoudi, 2021; Liu and Abbaszadeh, 2019) in that: (1) The research object of this paper is the simultaneous existence of multiple radioactive sources in the area. GEANT4 is used to approximate the energy deposition distribution of γ radioactive sources at different or the same location, and the SAW algorithm is used to extract the energy deposition values under different paths as the input data which are input into the designed neural network architecture for training. (2) In this paper, the cases that the radiation signal is blocked by the concrete walls are studied, and the effect of the walls of different geometries on the location estimation of multiple γ radioactive sources is tested. Experimental results show that the accuracy of the source location estimation decreases with the increase of wall length. The greater the number of walls, the more pronounced the decrease in the accuracy of source location estimation.

3. Radioactive source localization method

3.1. Problem description

For analysis conveniently, all unknown radioactive sources are regarded as point sources. Assuming that the size of the area where radioactive sources are located is 10 m by 10 m. The area is divided into 25 cells (the size of each cell is 2 m by 2 m), as shown in Fig. 1. It can be seen that the radioactive sources may appear anywhere in the area. To obtain an approximation of the energy deposition distribution in the area where radioactive sources are located, the energy deposition distribution is simulated by Geant4, assuming that radioactive sources are located in the center of the cells. Geant4 can simulate and track particles of different energies in various materials by the Monte Carlo (MC) method, and is used to simulate the physical process of particle transport in matter. It is widely used in nuclear technology, nuclear physics, accelerator design and other fields. The energy deposition distribution of radioactive sources in the actual environment can be approximated by the Geant4 program (Agostinelli et al., 2003). Radioactive sources

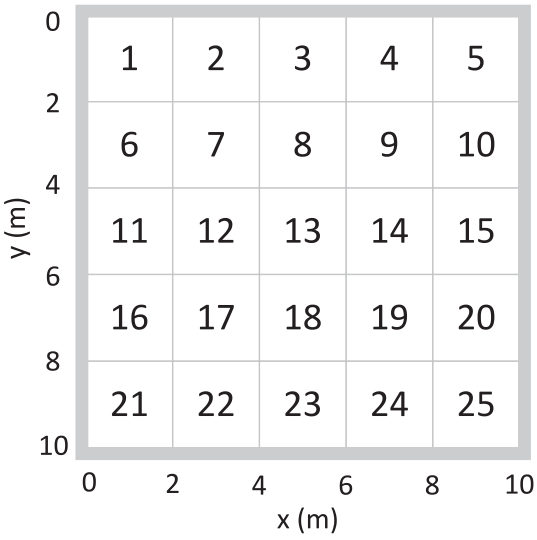

Fig. 1. An area consists of 25 cells. The grey area represents the boundary of the area where the radioactive sources are located.

mainly include α, β, γ and neutron sources according to the type of rays they emit. Due to the weak penetration of α and β rays, they are easily blocked by obstacles. The main research objects are γ and neutron radioactive sources (Al Hamrashdi et al., 2019). This paper mainly focuses on the localization of γ radioactive sources. Gamma rays emitted by γ radioactive sources which interact with matter mainly ionize via three processes: photoelectric effect, compton scattering and pair production. These processes can be defined in Geant4.

In the Geant4 program, we set both radioactive sources as γ radioactive sources with an energy of 1.33 MeV and an intensity of 2×10^6 CPS. In addition, each cell is again divided into 8 by 8 grids with an area of 0.25 m by 0.25 m. Since a single radioactive source may be in any of the 25 small units, the locations of two radioactive sources have $C_{25}^2 + C_{25}^1$ classifications in the area (each classification corresponds to two digital labels, and each digital label represents the location of a radioactive source in the area), as shown in Fig. 2. The energy deposition distribution of radioactive sources corresponding to all classification can be obtained through Geant4. The energy deposition distribution of two radioactive sources at different locations in the area is shown in Fig. 3.

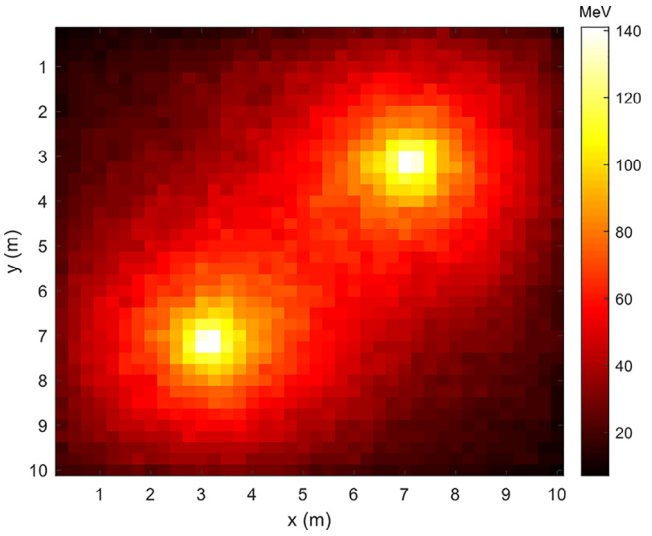

Fig. 3. Energy deposition distribution of two radioactive sources at different locations in the area.

3.2. SAW algorithm

In Section 3.1, a 40 × 40 energy deposition matrix was obtained. Next, the energy deposition values of 10 steps, 15 steps and 20 steps are collected from the 1600 grids respectively (each step represents one measurement of energy deposition within a grid) as the number of measurements in the radiation environment. It is then necessary to use SAW algorithm to move around the environment and collect energy deposition values.

The SAW algorithm does not repeat the path it has moved before (Brereton, 2014). In general, a common method for generating n-step paths is to randomly walk in the up, down, left, and right directions to determine the next position. The probability of walking in each direction is 1/4. (x_n, y_n) and (x_{n-1}, y_{n-1}) represent the coordinate positions of X_n and X_{n-1}, respectively, and $\{X_n\}_{n\geq 0}$. Then the probability of X_n is given by.

$$P(X_n = (x_n, y_n) | X_{n-1} = (x_{n-1}, y_{n-1})) = \begin{cases} 1/4, if |x_n - x_{n-1}| + |y_n - y_{n-1}| = 1 \\ 0, otherwise \end{cases} \tag{1}$$

However, for more steps, more computing resources need to be consumed to obtain a self-avoiding path. In order to improve the efficiency of generating self-avoiding path, a weighted importance sampling method is used for more steps (Bousquet-Mélou, 2014). Set a self-avoiding path: $X_0 = (x_0, y_0), X_1 = (x_1, y_1), \ldots, X_n = (x_n, y_n)$. Then the probability mass function can be obtained by importance sampling as:

$$P(X_0, X_1, ..., X_n) = \frac{I((X_0, X_1, ..., X_n) \in E_n)}{Z_n} \tag{2}$$

E_n is the set of n-step self-avoiding path and Z_n is unknown. A new probability mass function $Q(X_0, X_1, ..., X_n)$ is defined for weighted importance sampling. Let the number of unoccupied neighbors of X_{i-1} be d_{i-1}. Since all information before step i is known when estimating X_i, $Q(X_i | X_0, ..., X_{i-1})$ is given by.

$$Q(X_i | X_0, ..., X_{i-1}) = \begin{cases} 1/d_{i-1}, if\ X_i\ is\ unoccupied\ neighbor\ of\ X_{i-1} \\ 0, otherwise \end{cases} \tag{3}$$

and $X_0, X_1, \ldots, X_n$ will have a probability of

$$Q(X_0, X_1, ..., X_n) = \frac{I((X_0, X_1, ..., X_n) \in E_n)}{d_0 \cdots d_{i-1}} \tag{4}$$

Since $P(X_0, X_1, ..., X_n)$ is proportional to $I((X_0, X_1, ..., X_n) \in E_n)$, we can use the weight form as:

$$W(X_0, X_1, ..., X_n) = I((X_0, X_1, ..., X_n) \in E_n) d_0 \cdots d_{n-1}$$

The SAW algorithm that generates the measurement path is as follows:

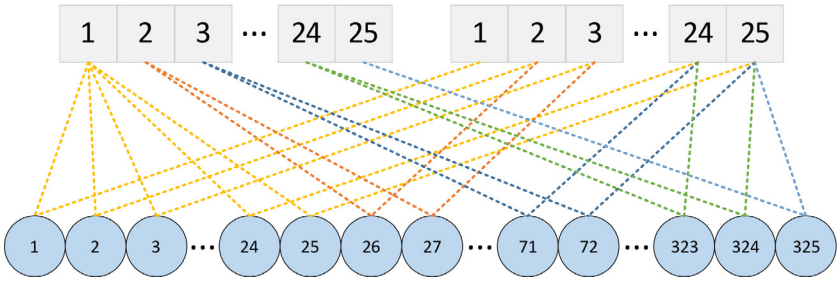

Fig. 2. Different locations of two radioactive sources in the area correspond to different digital labels.

Algorithm 1 Generate measurement path using SAW algorithm.

Input: energy deposition matrix A, n steps, step distance
While " generate number of steps is not n steps" **do**
  Randomly generate (x_0, y_0) as the starting point
  Generate a zeros matrix B of the same dimension as A
  Assign the row and column of matrix B corresponding to x_0 and y_0 to 1
  for i = 1,. . .,n **do**
    if " the number of unoccupied neighbors of X_i is not 0" **then**
      Update $W(X_0, X_1, ..., X_n)$ using Eq.(5)
      Assign $B(x_i, y_i)$ to 1
      if "exceeds matrix dimensions" or "(x_i, y_i) is at the wall position" **then**
        break;
  end for
end
Multiply the matrix A with the matrix B
Output: Matrix with measurement path

Fig. 4 shows that in the SAW algorithm, the number of steps of a self-avoiding path is set to 10, and the step distance is set to 0.5 m. The energy deposition values were collected at an interval of 0.5 m in order to reduce the number and time of measurements. Since the energy deposition values in the unmeasured grid are unknown, we set the energy deposition values in these grids to zero. Also, if there are walls inside the area, Algorithm 1 can automatically bypass the walls. Finally, the data containing measurement paths and measurement values are obtained by Algorithm 1. Next, we will feed the data into the CNN for pre-training.

3.3. The CNN architecture

CNN is mainly composed of input layer, convolution layer, pooling layer, fully connected layer and output layer (Russell, 2002). The input layer is generally a two-dimensional or three-dimensional array. The convolutional layer is mainly used to extract features from the input layer. Pooling layer can reduce the dimensionality of data by combining the outputs of neurons clusters in one layer into a single neuron in the next layer, avoiding overfitting. Limited by the valid values in the input data, pooling layer and padding are not used in this paper. The fully connected layer connects each neuron in one layer to each neuron in the next layer, and obtains the output by nonlinearly combining the extracted features. The downstream of the full connection layer is usually the output layer, which outputs the classification label in the multi-classification problems.

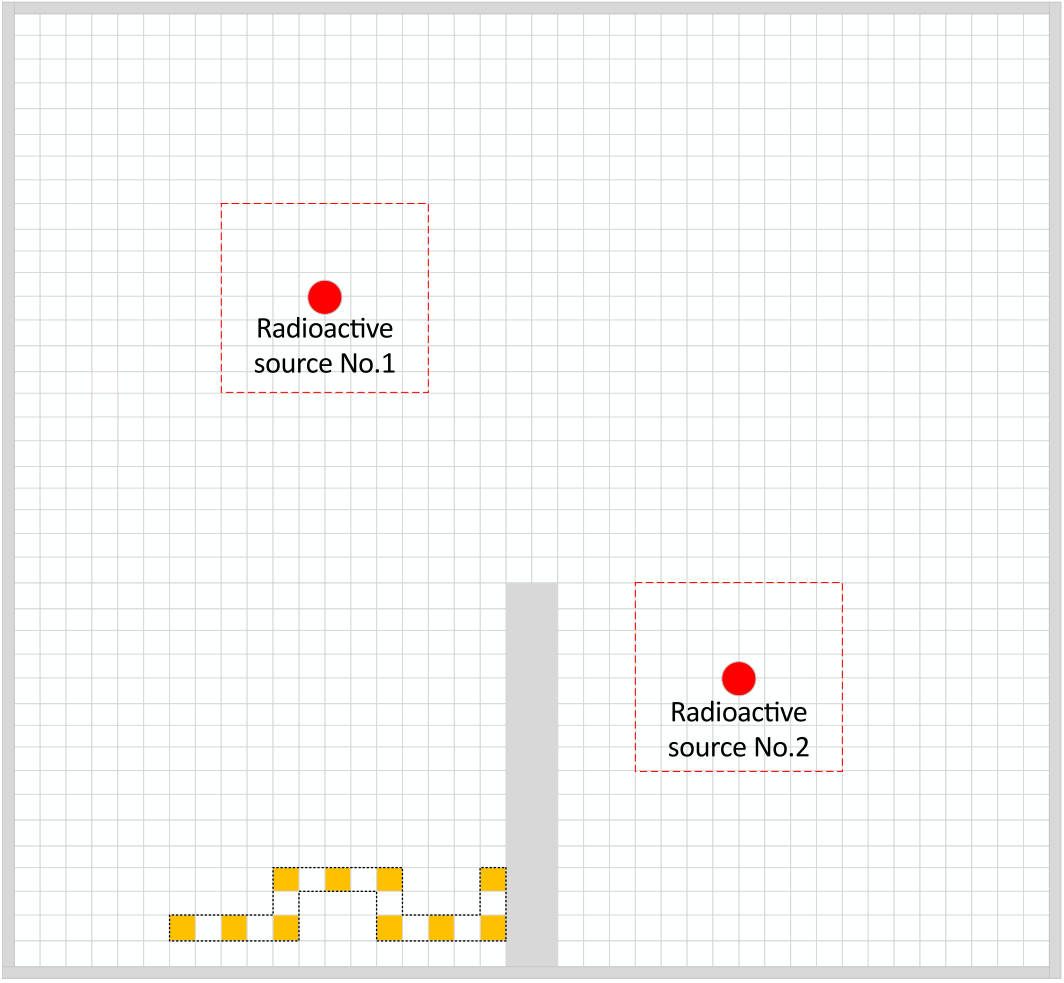

Fig. 4. The yellow grids represent the random walk measurement path, the gray area represents the boundary of the area and a wall inside the area, and the red boxes represent the area where radioactive sources are located. (For interpretation of the references to colour in this figure legend, the reader is referred to the web version of this article.)

In addition, both convolutional layers and fully connected layers introduce nonlinear activation functions (Glorot et al., 2011). The ReLu activation function has the functions of preventing gradient dispersion, sparse activation and efficient calculation, and is better able to train deeper networks. The ReLu activation function is defined as $f(x) = max(0, x)$. In multinomial logistic regression, Softmax is generally used as the last activation function of the neural network. The loss function generally adopts the cross-entropy loss function (LeCun et al., 1998; Krizhevsky et al., 2012; Simonyan and Zisserman, 2014), which normalizes the output of the network to the probability distribution of the output category. The Softmax activation function is defined as $Softmax(x_i) = \frac{e^{x_i}}{\sum_{j=1}^{k} e^{x_j}}$. The cross-entropy loss function is defined as $J = -\sum_{i=1}^{K} y_i log(p_i)$. Where K is the number of classifications; y_i is the classification label; p_i is the probability of the corresponding category i.

In addition to determining the activation function, other hyperparameters also need to be set during model training, including the size of the convolution kernel, the number of neural network layers, the number of neurons in the fully connected layer, the optimizer category, the batch-size, and epoch (Tan and Le, 2019; Smith, 2018). These hyperparameters are derived from engineering experience. The settings of the CNN hyperparameters in this paper are shown in Table 1.

The energy deposition dataset containing the measurement paths and measurement values obtained in Section 3.2 is divided into three parts: training set, validation set and test set. The dataset is randomly divided into proportions; the training set is 98% of the dataset; the validation set is 1% of the dataset; the test set is 1% of the dataset. According to the division of the dataset, we design the CNN architecture as shown in Fig. 5. The first layer is the input layer, and the input data are expanded into three-channel. The convolution kernel size of the convolutional layer Conv1 is 3 × 3, and the number of channels is 32. The convolution kernel size of the convolutional layers Conv2 and Conv3 is also 3 × 3, but the number of channels is 64. FC4, FC5 and FC6 are fully connected layers, and the number of neurons in each layer is 1000, 400 and 325 respectively. The 325 nodes represent 325 classification labels respectively, and each classification label corresponds to the respective locations of two radioactive sources in the area. The activation functions of the convolutional layers Conv1, Conv2, Conv3 and the fully connected layers FC4 and FC5 all use the ReLu activation function. The activation function of the output layer FC6 uses the Softmax activation function.

Table 1
The CNN hyperparameters.

Hyperparameter	Selection	Description
Convolution kernel	3 × 3	Convolution kernel size of CNN
Neural network layer	7	The number of layers in CNN
Neuron	1000,400,325 respectively	The number of neurons in the fully connected layer
Optimizer	Adam	Optimizer for CNN
Batch-size	16	The size of each batch of data
Epoch	25	The number of training times for all samples in the training set

4. Experimental results and analysis

In order to verify the rationality and correctness of the method proposed in this paper, the experiments for estimating the location of two radioactive sources are carried out under the condition of no obstacles and complex obstacles. In addition, we also conduct experiments for estimating the location of three radioactive sources in a restricted area.

4.1. Experimental analysis without obstacles

We set the number of steps to 10 steps and the step distance to 0.5 m, generating 1,300,000 data. The generated data is input into the CNN architecture in Fig. 5 for training. Both training accuracy and training loss have converged after 25 epochs. The curves of training accuracy, validation accuracy, training loss, and validation loss are shown in Fig. 6. The expected training result is that the validation accuracy is as large as possible, and the validation loss is as small as possible, close to the training loss.

At the same time, we explore the impact of different dataset sizes on validation accuracy. 1,625,000 and 1,950,000 data are respectively input into the CNN architecture for training, and the training results are shown in Figs. 7 and 8. As shown in Fig. 7, with the increase of the input data, the validation accuracy is continuously increasing. Comparing Fig. 8 with Fig. 6, it can be seen that with the increase of the dataset size, the validation accuracy gradually increases and the validation loss gradually decreases.

Besides, we also explore the impact of different steps on validation accuracy. We set the number of steps to 15 steps, and the step distance remains the same. 1,300,000, 1,625,000, and 1,950,000 data are generated and respectively fed into the CNN architecture

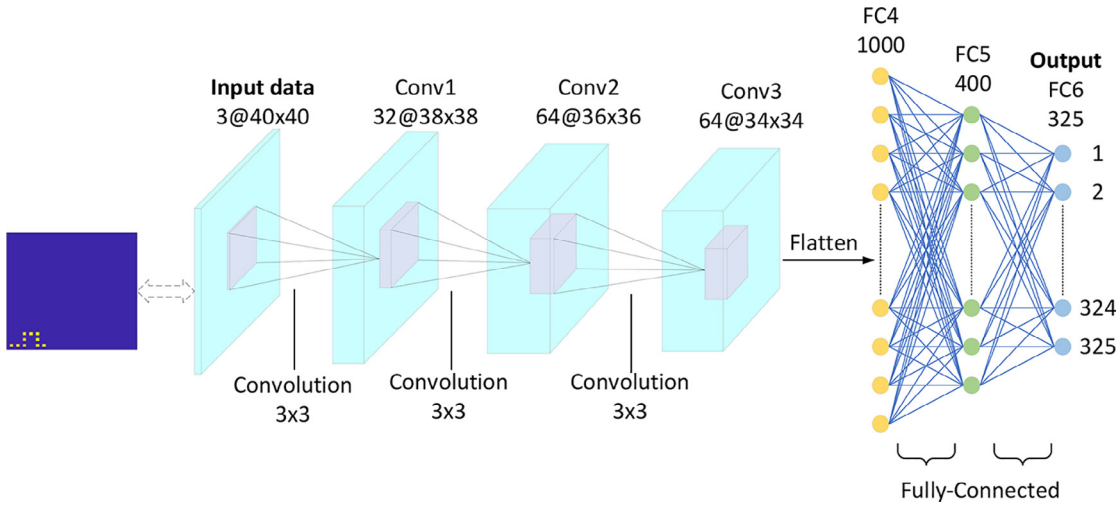

Fig. 5. Schematic illustration of the CNN architecture. Conv1, Conv2 and Conv3 represent convolutional layers, and FC4, FC5 and FC6 represent fully connected layers.

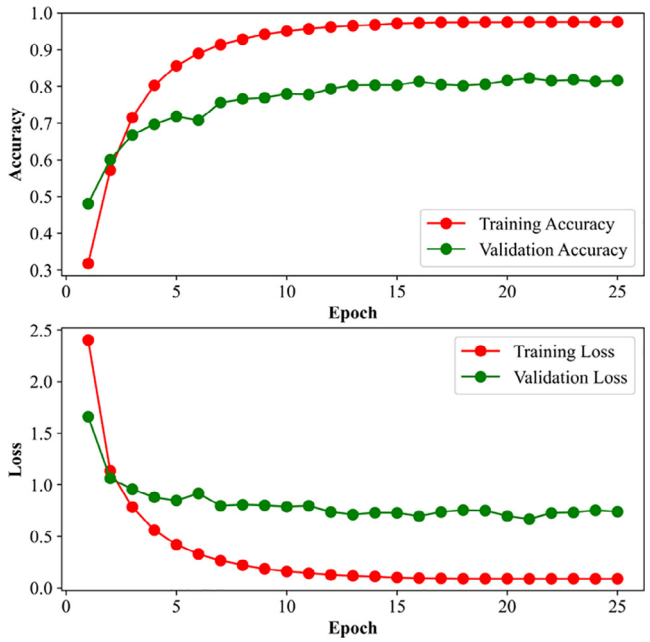

Fig. 6. CNN training results with 10 steps and the dataset size is 1,300,000.

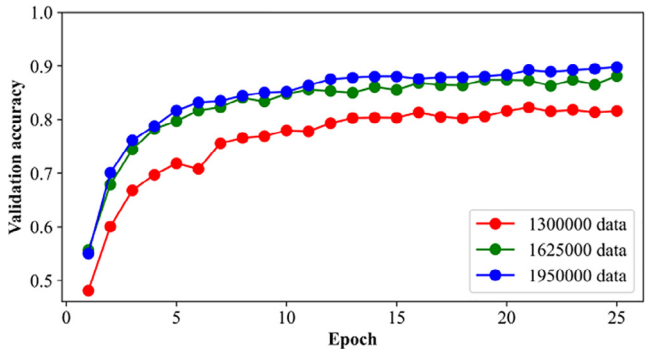

Fig. 7. CNN training results with 10 steps and the dataset sizes are 1,300,000, 1,625,000, and 1,950,000, respectively.

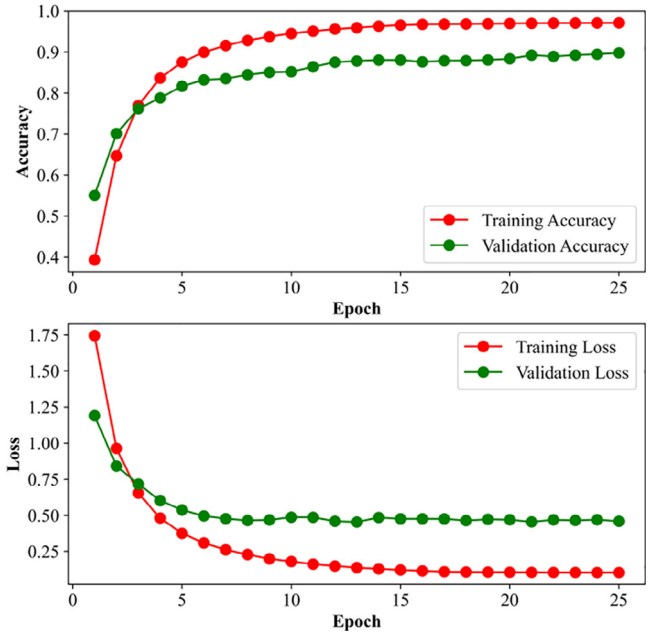

Fig. 8. CNN training results with 10 steps and the dataset size is 1,950,000.

for training. After 25 epochs, the respective validation accuracy and validation loss are obtained as shown in Fig. 9 (a). Then set the number of steps to 20 steps. Similarly, the training accuracy, validation accuracy, training loss, and validation loss are obtained after 25 epochs as shown in Fig. 9 (b). Comparing (a) and (b) of Fig. 9, it can be seen that as the number of steps increases, the validation accuracy is continuously increasing and the validation loss is continuously decreasing.

To evaluate the performance of the CNN model, we input new data (test set, 1% of the dataset) into the trained model. Two important parameters are used to evaluate the performance of the CNN model: precision and accuracy. Precision represents the proportion of correct detection by the model. Accuracy represents how accurately the model predicts new data. The test data of 10, 15, and 20 steps are respectively input into the trained CNN model. The performance evaluation of the CNN model is shown in Table 2. The results in Table 2 show that when the input data is 1,950,000, the accuracy of the network model for 10 measurements of energy deposition is 89%. Compared with 10 measurements, the accuracy of the network model with 15 measurements and 20 measurements increases by 4.4% and 7.2%, respectively. However, when the size of the input dataset exceeds 1,950,000, the accuracy will not be significantly improved and the training time will be greatly increased. In addition, while 15 or 20 measurements of energy deposition are more accurate, the more measurements in the radiation area, the longer it takes. In order to complete the localization of two radioactive sources in less time, it is more appropriate to select 10 measurements of energy deposition to locate two radioactive sources in the radiation environment.

4.2. Experimental analysis of obstacle existence

(1) The case of a single wall inside the area

Suppose that there is one wall inside the area, the width of the wall is 50 cm, and the length of the wall is set to 2 m, 4 m, 6 m and 8 m, respectively. Two radioactive sources are randomly distributed at different locations in the area. Fig. 10 shows the energy deposition distribution of two radioactive sources with one wall inside the area (ignore energy deposition within wall). Then set the number of steps to 10, and input 1,950,000 data corresponding to the steps into the neural network for training. The training results are shown in Fig. 11.

In order to evaluate the performance of the network model when there is one wall inside the area, we input the test data into the trained network model. The performance evaluation of the network model is shown in Table 3. The results show that two radioactive source locations can be estimated simultaneously with 92% accuracy when there is one 2 m long wall inside the area. But as the wall length increases, the accuracy gradually reduces. Compared with the 2 m long wall, the accuracy of the 4 m, 6 m, and 8 m long wall is reduced by 2.0%, 4.1%, and 8.3%, respectively. When there is one 8 m long wall inside the area, two radioactive source locations can be estimated with 85% accuracy.

(2) The case of two walls inside the area

Suppose that there are two walls inside the area, and the length of the two walls is set to 2 m, 4 m, 6 m and 8 m, respectively. Fig. 12 shows the energy deposition distribution of the radioactive sources with two overlapping walls (6 m) inside the area. Analogously, the number of steps is set to 10. Then 1,950,000 data generated by Algorithm 1 are input into CNN. The training results are shown in Fig. 13.

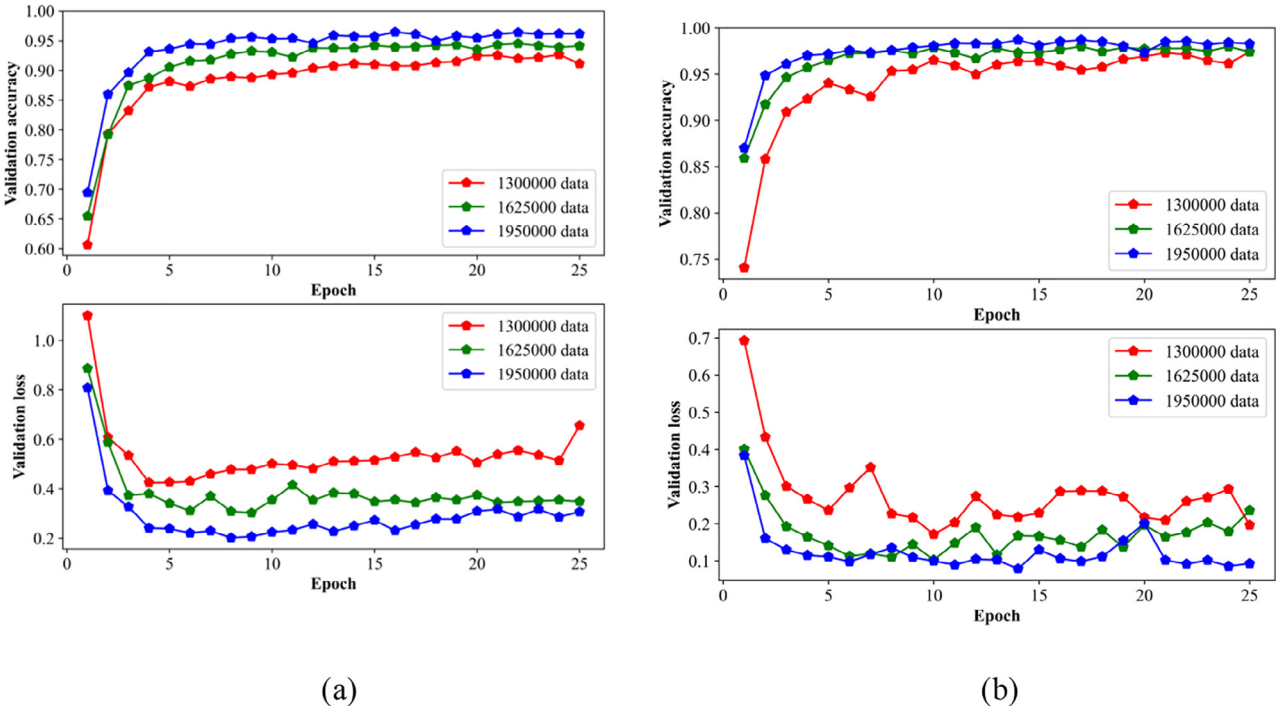

Fig. 9. The dataset size is 1,300,000, 1,625,000, and 1,950,000, respectively. (a) The number of steps is 15 to obtain the respective validation accuracy and validation loss curves. (b) The number of steps is 20 to obtain the respective validation accuracy and validation loss curves.

Table 2
Performance evaluation of CNN model when there are no obstacles in the area.

The number of steps	Dataset size	Precision	Accuracy
10	1,300,000	0.8159	0.8104
10	1,625,000	0.8812	0.8811
10	1,950,000	0.8980	**0.8924**
15	1,300,000	0.9065	0.9013
15	1,625,000	0.9136	0.9128
15	1,950,000	0.9338	0.9315
20	1,300,000	0.9441	0.9440
20	1,625,000	0.9499	0.9482
20	1,950,000	0.9570	0.9568

We input the test data into the network model for evaluation, and the performance evaluation of the network model is shown in Table 3. The results show that when the length of two walls is 2 m or 4 m, the accuracy is similar to that of one wall of the same length. However, when the length of the two walls is 6 m or 8 m, the accuracy is greatly reduced compared to an area with only one wall of the same length. When the length of two walls is increased to 8 m, the accuracy is 68%.

4.3. Simultaneous localization of three radioactive sources

In Sections 4.1 and 4.2, we study how to simultaneously locate two radioactive sources in the area, and the experimental results

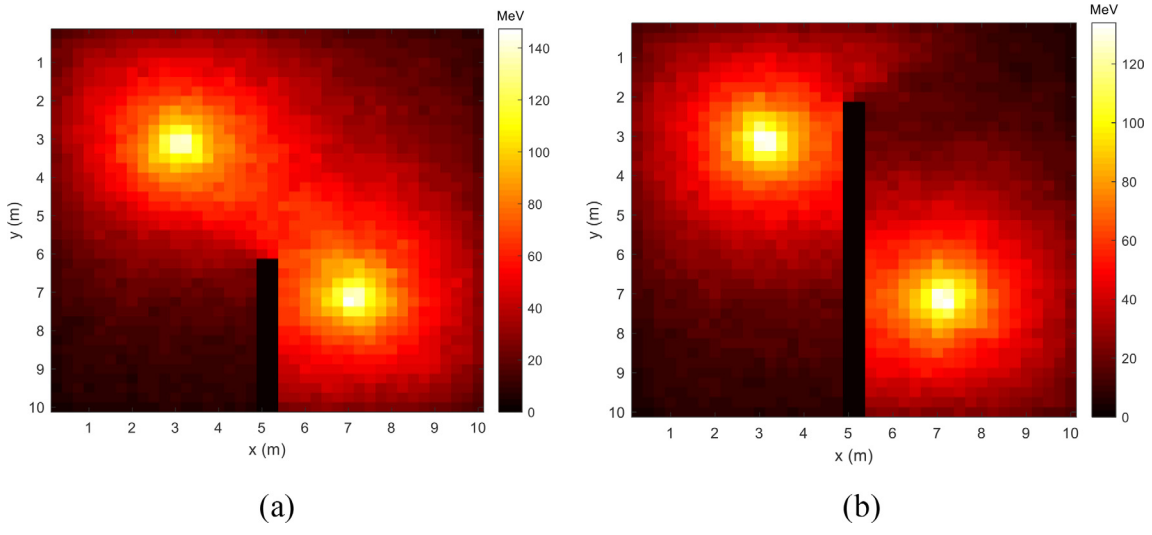

Fig. 10. Energy deposition distribution of two radioactive sources. The black area represents the location of the wall. (a) One 4 m long wall inside the area. (b) One 8 m long wall inside the area.

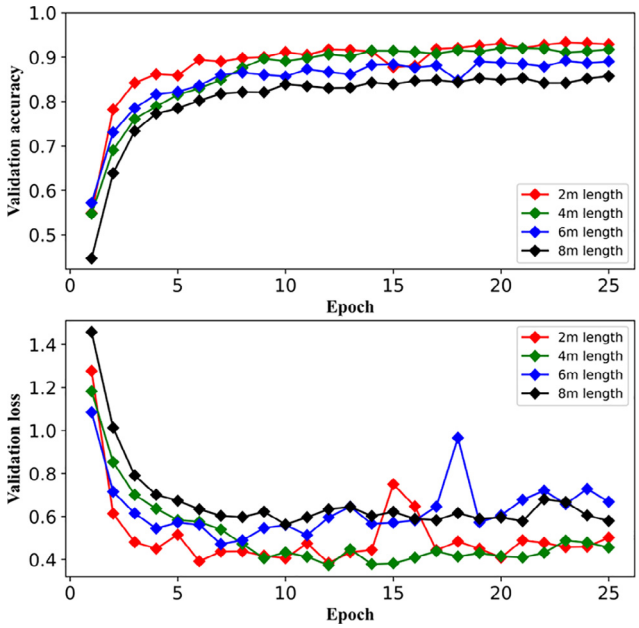

Fig. 11. The respective validation accuracy and validation loss curves. There is one wall inside the area, and the length of the wall is 2 m, 4 m, 6 m and 8 m, respectively.

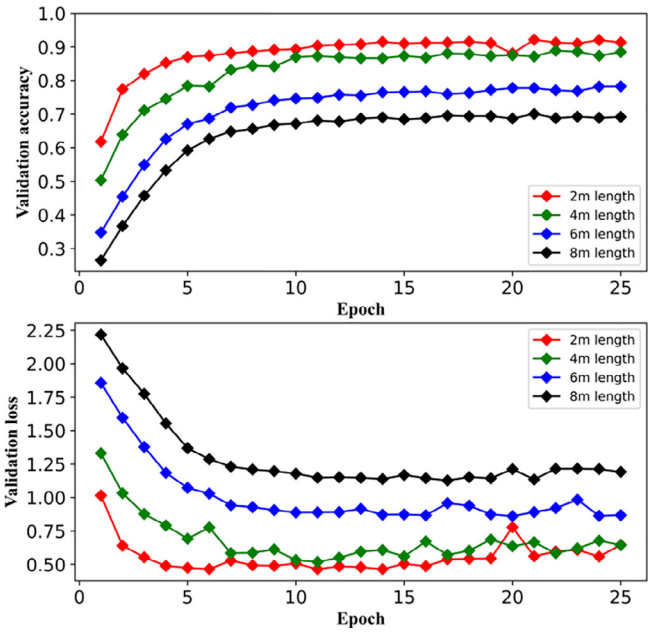

Fig. 13. The respective validation accuracy and validation loss curves. The length of the two walls is 2 m, 4 m, 6 m and 8 m, respectively.

Table 3
Performance evaluation of CNN model when there are obstacles in the area.

The length of wall	One wall		Two wall	
	Precision	Accuracy	Precision	Accuracy
2 m	0.9332	0.9289	0.9205	0.9132
4 m	0.9172	0.9103	0.8890	0.8844
6 m	0.8918	0.8904	0.7995	0.7926
8 m	0.8573	**0.8518**	0.7010	**0.6860**

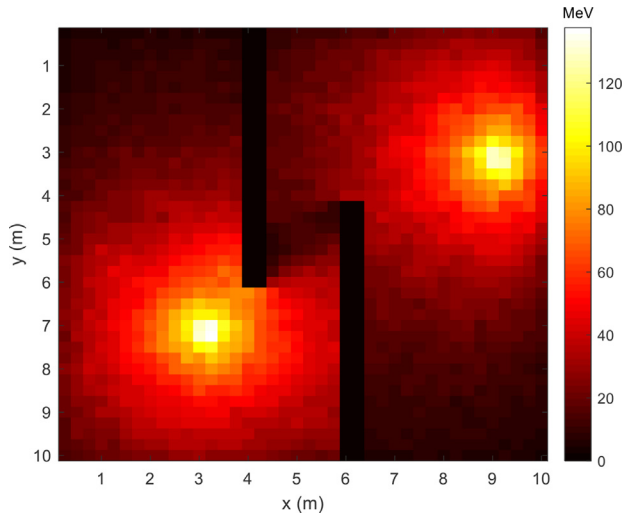

Fig. 12. Energy deposition distribution of the radioactive sources when there are two overlapping long walls inside the area.

show that the proposed method can solve the problem of localizing multiple radioactive sources in the radiation area. In order to further verify the feasibility of the proposed method, we add another radioactive source (the energy is 1.33 MeV and the intensity is 2×10^6 CPS) to explore the localization of three unknown radioactive sources in the area. It is more challenging to locate three radioactive sources simultaneously than to locate a single radioactive source or two radioactive sources. The location distribution of three radioactive sources in the area can be subdivided into the following three situations:

(1) Three radioactive sources are distributed at different locations in the area.
(2) Two radioactive sources are in the same location, but another is in a different location.
(3) Three radioactive sources in the same location in the area.

To facilitate the experimental study, we assume that three radioactive sources are distributed only in the middle of the area (6 m by 6 m). According to the cell and grid division method in Section 3.1, there are 165 location classifications for three radioactive sources in this area. The energy deposition distribution of radioactive sources corresponding to each location classification is approximated by Geant4 (Fig. 14). Then set the number of steps to 10 and the step distance to 0.5 m to complete ten measurements of energy deposition. Next, 825,000, 990,000 and 1,155,000 data, including measurement paths and measurement values, are generated respectively by algorithm 1.

Since the dimension of the input data changes, the CNN architecture also needs to be adjusted appropriately. The number of neurons in the three fully connected layers (FC4, FC5 and FC6) in Fig. 5 is adjusted to 500, 300 and 165, respectively. The rest of architecture and hyperparameters of the neural network remain unchanged. Input the collected data (825,000, 990,000, 1,155,000) into the CNN for training. Then the validation accuracy and validation loss curve obtained by training are shown in Fig. 15. It can be seen that as the size of the dataset increases, the validation accuracy keeps increasing and the validation loss keeps decreasing. The test data is then fed into the trained network model. The prediction accuracy of the network model is 0.8648, 0.8968, and 0.9166, respectively. Therefore, by properly tuning the hyperparameters of the fully connected layers, the

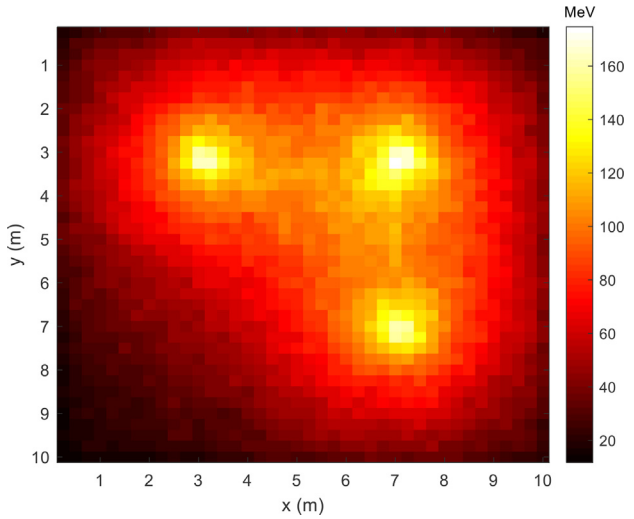

Fig. 14. Energy deposition distribution of three radioactive sources at different locations in the area.

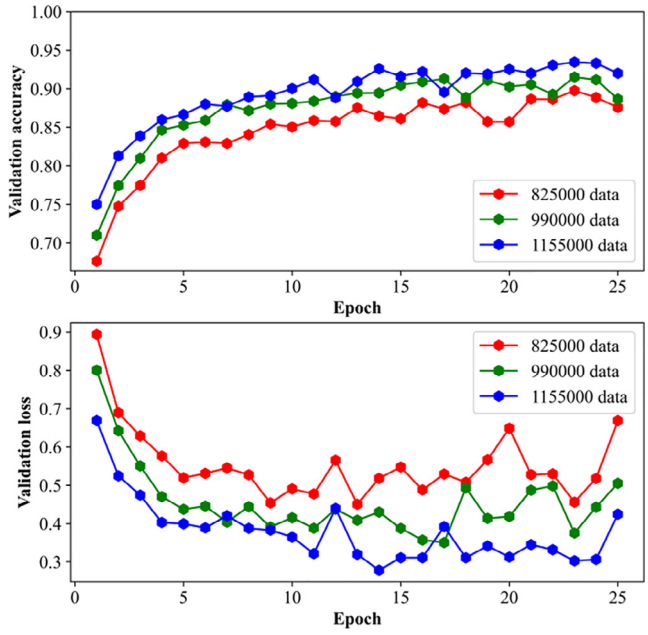

Fig. 15. The respective validation accuracy and validation loss curves for different dataset sizes.

CNN architecture is equally suitable for locating three radioactive sources. However, when considering locating more radioactive sources simultaneously in the radiation area, the divided cells may have to be reduced to achieve higher prediction accuracy.

5. Conclusion

In order to quickly locate the multiple unknown radioactive sources in the area, a method combining SAW and CNN algorithms is proposed in this paper. The area where two unknown gamma radioactive sources are located is divided into cells of the same size, with a total of 325 classifications for source locations. The energy deposition distribution of gamma radioactive sources in the area is obtained by Geant4 simulation. Then, the energy deposition values in the area are randomly collected by the SAW algorithm, and three datasets of training, validation and test are constructed. The collected data are trained and analyzed by CNN to predict respective locations of unknown radioactive sources. The experimental results show that by ten measurements (energy deposition) in an unobstructed area, the network model can predict the respective locations of two radioactive sources with an accuracy of 89%. The respective locations of two radioactive sources can be predicted with 68% accuracy in the case of complex obstacles. Additionally, the CNN architecture adjusted appropriately can also be applied to locate three radioactive sources.

This paper demonstrates the feasibility of combining SAW and CNN algorithms in solving the localization problem of multiple unknown radioactive sources. In the future, we are going to carry out some work to improve the localization task of radioactive sources. On the one hand, we need to consider the effect of background dose in the environment on the accuracy of radioactive sources localization. On the other hand, real-world application scenarios that are more complex than the simulation environment, such as terrain constraints, also need to be considered. In addition, the method proposed in this paper has certain limitations when the number of radioactive sources is unknown in the area. In order to solve the problem of radioactive source localization better, it may be necessary to combine other methods such as particle filtering and reinforcement learning.

CRediT authorship contribution statement

Xulin Hu: Methodology, Writing – original draft, Software. **Jianwen Huo:** Conceptualization, Methodology, Software. **Junling Wang:** Visualization, Investigation. **Li Hu:** Validation, Supervision. **Yufeng Xiao:** Writing, reviewing & editing.

Data availability

No data was used for the research described in the article.

Declaration of Competing Interest

The authors declare that they have no known competing financial interests or personal relationships that could have appeared to influence the work reported in this paper.

Acknowledgments

This research was funded by the National Natural Science Foundation of China (No.12175187), National Key R&D Program of China (NO.2021YFB1715000), Sichuan Science and Technology Program (NO.2022YFG0242) and NHC Key Laboratory of Nuclear Technology Medical Transformation (MIANYANG CENTRAL HOSPITAL) (No.2021HYX16).

References

IAEA Incident and Trafficking Database (ITDB), Incidents of Nuclear and Other Radioactive Material out of Regulatory Control. Available online: https://www.iaea.org/sites/default/fifiles/20/02/itdb-factsheet-2020.pdf (accessed on 13 February 2020).

Kamiya, K., Ozasa, K., Akiba, S., Niwa, O., Kodama, K., Takamura, N., Zaharieva, E.K., Kimura, Y., Wakeford, R., 2015. Long-term effects of radiation exposure on health. Lancet 386 (9992), 469–478.

Morelande, M., Ristic, B., Gunatilaka, A., 2007. Detection and parameter estimation of multiple radioactive sources. Proceedings of the 10th International Conference on Information Fusion.

Chao, N., Liu, Y., Xia, H., Peng, M.J., Ayodeji, A., 2019. DL-RRT* algorithm for least dose path Re-planning in dynamic radioactive environments. Nucl. Eng. Technol. 51 (3), 825–836.

Liu, A.H.W., 2010. Simulation and implementation of distributed sensor network for radiation detection. California Institute of Technology.

Chin, J.C., Rao, N., Yau, D., Shankar, M., Yang, Y., Hou, J.C., Srivathsan, S., Iyengar, S., 2008. Identification of low-level point radiation sources using a sensor network. 2008 International conference on information processing in sensor networks, IEEE.
Gunatilaka, A., Ristic, B., Gailis, R., 2007. On localisation of a radiological point source. Information, Decision and Control, IEEE.
Howse, J.W., Ticknor, L.O., Muske, K.R., 2001. Least squares estimation techniques for position tracking of radioactive sources. Automatica 37 (11), 1727–1737.
Bai, E.W., Heifetz, A., Raptis, P., Dasgupta, S., Mudumbai, R., 2007. Maximum likelihood localization of radioactive sources against a highly fluctuating background. Decision and Control, IEEE.
Chandy, M., Pilotto, C., McLean, R., 2008. Networked sensing systems for detecting people carrying radioactive material. Proceedings of the INSS 5th International Conference on Networked Sensing Systems.
Liu, A.H., Bunn, J.J., Chandy, K.M., 2011. Sensor networks for the detection and tracking of radiation and other threats in cities. Proceedings of the 10th International Conference on Information Processing in Sensor Networks (IPSN).
Morelande, M.R., Ristic, B., 2009. Radiological source detection and localisation using Bayesian techniques. IEEE Trans. Signal Process. 57 (11), 4220–4231.
Huo, J., Liu, M., Neusypin, K.A., Liu, H., Guo, M., Xiao, Y., 2020. Autonomous Search of Radioactive Sources through Mobile Robots. Sensors 20 (12), 3461.
Ling, M., Huo, J., Moiseev, G.V., Hu, L., Xiao, Y., 2022. Multi-robot collaborative radioactive source search based on particle fusion and adaptive step size. Ann. Nucl. Energy 173, 109104.
Gao, W., Wang, W., Zhu, H., Huang, G., Wu, D., Du, Z., 2018. Robust radiation sources localization based on the peak suppressed particle filter for mixed multi-modal environments. Sensors 18 (11), 3784.
Lee M S., Hanczor, M., Chu, J., He, Z., Michael, N., Whittaker, R., 2018. 3-d volumetric gamma-ray imaging and source localization with a mobile robot. arXiv preprint arXiv:1802.06072.
Liu, R., Koch, A., Zell, A., 2013. Mapping UHF RFID tags with a mobile robot using a 3D sensor model. IEEE/RSJ International Conference on Intelligent Robots & Systems. IEEE.
Liu, R., Huskić, G., Zell, A., 2015. On tracking dynamic objects with long range passive UHF RFID using a mobile robot. Int. J. Distrib. Sens. Netw. 11, (5) 781380.
Hata, H., Yokoyama, K., Ishimori, Y., Ohara, Y., Tanaka, Y., Sugitsue, N., 2015. Application of support vector machine to rapid classification of uranium waste drums using low-resolution γ-ray spectra. Appl. Radiat. Isot. 104, 143–146.
Bobin, C., Bichler, O., Lourenço, V., Thiam, C., Thévenin, M., 2016. Real-time radionuclide identification in γ-emitter mixtures based on spiking neural network. Appl. Radiat. Isot. 109, 405–409.
Fathi, A., Masoudi, S.F., 2021. Lost gamma source detection algorithm based on convolutional neural network. Nucl. Eng. Technol. 53 (11), 3764–3771.
Liu, Z., Abbaszadeh, S., 2019. Double Q-learning for radiation source detection. Sensors 19 (4), 960.
Agostinelli, S., Allison, J., Amako, K.A., Apostolakis, J., Araujo, H., Arce, P., 2003. GEANT4—a simulation toolkit. Nucl. Instrum. Methods Phys. Res., Sect. A 506 (3), 250–303.
Al Hamrashdi, H., Monk, S.D., Cheneler, D., 2019. Passive gamma-ray and neutron imaging systems for national security and nuclear non-proliferation in controlled and uncontrolled detection areas: Review of past and current status. Sensors 19 (11), 2638.
Brereton, T., 2014. Stochastic Simulation of Processes, Fields and Structures. Institute of Stochastic.
Bousquet-Mélou, M., 2014. On the importance sampling of self-avoiding walks. Comb. Probab. Comput. 23 (5), 725–748.
Russell, Stuart, J., 2002. Artificial intelligence: a modern approach.
Glorot, X., Bordes, A., Bengio, Y., 2011. Deep sparse rectifier neural networks. J. Mach. Learn. Res. 15, 315–323.
LeCun, Y., Bottou, L., Bengio, Y., Haffner, P., 1998. Gradient-based learning applied to document recognition. Proc. IEEE 86 (11), 2278–2324.
Krizhevsky, A., Sutskever, I., Hinton, G.E., 2012. Imagenet classification with deep convolutional neural networks. Adv. Neural Inf. Process. Syst.
Simonyan, K., Zisserman, A., 2014. Very deep convolutional networks for large-scale image recognition. arXiv preprint arXiv:1409.1556.
Tan, M., Le, Q., 2019. Efficientnet: Rethinking model scaling for convolutional neural networks. Int. Conf. Mach. Learn. PMLR 2019, 6105–6114.
Smith, L.N., 2018. A disciplined approach to neural network hyper-parameters: Part 1–learning rate, batch size, momentum, and weight decay. arXiv preprint arXiv:1803.09820.